Turk J Elec Eng & Comp Sci, Vol.18, No.6, 2010, © TÜBİTAK
doi:10.3906/elk-0911-295

Design and evaluation of a linear switched reluctance actuator for positioning tasks

António Eduardo Vitória do ESPÍRITO SANTO, Maria do Rosário CALADO, Carlos Manuel Pereira CABRITA
Department of Electromechanical Engineering, University of Beira Interior, 6201-001 Covilhã-PORTUGAL
e-mail: aes@ubi.pt, rc@ubi.pt, cabrita@ubi.pt

Abstract

This paper presents the development of a new linear switched reluctance actuator and confirms its applicability to perform positioning tasks. After the explanation of the actuator working principle and the presentation of its electromechanical topology, an analysis is accomplished using a finite elements tool. Based on the theoretical results, an experimental prototype that can develop 150 N was constructed. Its behaviour is observed under two different control methods implemented with microcontrollers. Initially, position is controlled applying a single pulse-driving scheme. Meanwhile, significant improvements are obtained with the introduction of a sliding-mode controller, allowing movements with 1 mm of resolution.

Key Words: *Actuator design, linear switched reluctance, position control, sliding mode*

1. Introduction

The development of linear actuators is today a research field of interest to the scientific community. Usually, rotating-to-linear motion conversion is achieved through mechanical gears. Since this solution is essentially mechanical, a special maintenance must be performed periodically, if high reliability and operational ability are demanded. This and others drawbacks, like space or efficiency, can be overstepped with the introduction of linear drives. Research is today focused in the investigation of new materials and technologies with the ability to directly produce a linear displacement and, simultaneously, is also trying to solve new problems directly related with linear actuators like the cogging force, the attractive force perpendicular to the movement, or the end effects. A survey of the different methods and their commercial application is made in [1], with special emphasis in magnetic devices. This paper proposes and presents a linear switched reluctance actuator and evaluates its performance and applicability in positioning tasks.

Various materials have been successfully used to convert electrical energy to mechanical effect; materials such as piezoelectric ceramics, polymers, and shape memory alloys are among the most widely used [2–4].

However, each one of these materials has limitations that interfere with its generalized application. Piezoelectric ceramics, like the PZT (Lead Zirconium Titanate), are limited to short amplitude movements, limiting its usage in situations where large amplitude movements are demanded. PVDF (Polyvinylidene Difluoride) is an electro-active polymer that, like piezoelectric ceramics, can only develop short amplitude movements. Alloy materials, like the Nitinol, can develop larger forces, with larger amplitudes but, unfortunately, its efficiency is poor and has slow dynamic response. Moreover, fabrication costs are prohibitive and production is usually complex.

An alternative solution to the previous materials is the force developed when using the electrostatic principle. The production techniques developed to the semiconductors fabrication can be applied to build small electrostatic actuators [5, 6].

Non-magnetic technologies, based either in new materials or physical principles, allow the fabrication of small dimensions actuators. The previously mentioned driving mechanisms are widely used to build small amplitude movement actuators with low force requirements. Solutions developed to perform high amplitude movements and forces, like public transportation systems, launchers, roller coasters, conveyors, robotics, high precision manufacturing systems, or small stroke devices, are normally based on magnetic technologies. Although they have low manufacturing costs, it is difficult to downsize their dimensions without losing performance.

An induction linear actuator has been proposed by [7] and is based on the same working principle as its rotating counterpart. For the past few years, the permanent magnets actuators have appeared [8, 9], regardless of their high costs. This technology was first applied to rotating actuators, but now it is also used to build linear drives.

In the two last decades the reluctance principle has emerged as an alternative. Linear switched reluctance (LSR) actuators exhibit high force/weight ratio, without the need of permanent magnets. Its structural complexity is low, allowing attractive manufacturing cost and high operation reliability, turning it suitable for traction force application [10, 11]. The major problem concerns development and implementation of an adequate control strategy that provides the required actuator operation. It also requires a power converter that feeds each one of the LSR actuator phases. Finally, one of the most common complaints against the LSR actuator is the acoustic noise produced under normal operation [12], as it is for the rotating switched reluctance machine [13].

The switched reluctance (SR) drives demand a command scheme that, sequentially, energises actuator phases. Different control solutions can be found in the literature. The fuzzy controller proposed in [14] controls the actuator velocity via modification of the turn-on angle, holding the turn-off angle depending on the velocity. The binary state is controlled in [15] with a fuzzy controller acting on parameters such as turn on and off angles, phase currents, and power source voltage. Another topic under research is the binary fluctuation; in [16] a solution based on fuzzy logic is proposed which controls the phase currents through an iterative method. All above-mentioned works are dedicated to the rotary machine, and largely focused in traction force application. Work addressing linear drives are also related to traction applications [17, 18]. In [19, 20] the authors propose also LSR actuators that can develop small displacements.

The remainder of this paper is organized as follows. An overview of the theoretical aspects related with the proposed LSR actuator is presented in section 2, followed by a presentation of its physical structure. A finite element tool is used in Section 3 to analyse and obtain the characteristic data of the actuator, such as traction force, attraction force, energy and co-energy. Section 4 presents the power converter used to feed

actuator phases. Two different control mechanisms are proposed and experimentally verified in Section 5 and the obtained results are presented and discussed. Finally, in Section 6 conclusions are drawn.

2. LSRA working principle

Magnetic reluctance is a measure of the opposition to the magnetic flux crossing of a magnetic circuit. If one of the magnetic circuit parts is allowed to move, then, system will try to reconfigure itself for a geometrical shape that corresponds to the minimal magnetic reluctance. Figure 1 illustrates the different stages associated with the energy conversion procedure, when a very fast movement from position x to position $x + \mathrm{d}x$ occurs.

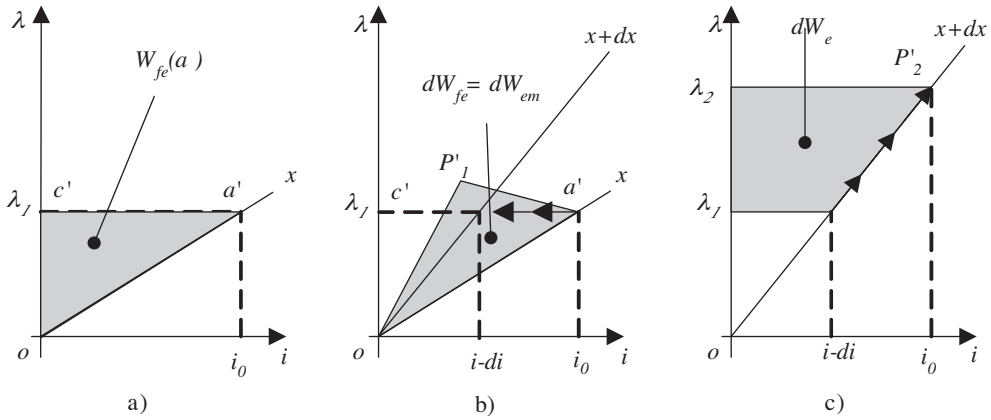

Figure 1. Quasi-instantaneous movement from position x to position $x + dx$: a) initial system condition, b) actuator movement, c) restoring energy.

It is assumed that motion occurs without a change in the linkage flux. At the beginning, the system energy W_{fe} is given by the area defined in Figure 1(a), that is

$$W_{fe}(a') = \text{area}\,\{o, a', c', o\}\,. \tag{1}$$

With actuator fast displacement from position x to position $x+dx$, as shown in Figure 1(b), some of the energy stored in the magnetic coupling field is converted into mechanical energy. This amount of energy is equivalent to the area given by

$$dW_{fe} = \text{area}\,\{o, a', P_1', o\}\,. \tag{2}$$

It can be observed that the energy stored in the coupling field decreases. Simultaneously, current also decreases. If voltage from the supply source is constant, the current will return to its initial value i_0, through the path represented in Figure 1(c), restoring the energy taken from the magnetic coupling field during the fast movement.

Since linkage flux is constant throughout the course of the movement, there is no induced voltage and, therefore, the magnetic coupling field does not couple energy from the voltage source.

An electromagnetic device can convert electrical energy into mechanical energy, or vice-versa. This process is made through the device magnetic field. The energy responsible for the actuator motion, promoted by the mechanical force f_{em} under a constant linkage flux λ, taken from the magnetic coupling field, is expressed by

the relationship

$$dW_{em} = -dW_{fe} \Rightarrow f_{em} = -\left.\frac{dW_{fe}}{dx}\right|_{\lambda=\text{constant}}. \tag{3}$$

Variation of the energy coupling field is equal, but with opposite signal, to the mechanical energy used to move the actuator. The mechanical force f_{em} can now be represented by the relation

$$W_{fe} = \frac{1}{2}\frac{\lambda^2}{L} \Rightarrow f_{em} = \frac{\lambda^2}{2L^2}\frac{dL}{dx} = \frac{i^2 dL}{2dx}. \tag{4}$$

Since i^2 is always positive, the force applied to the actuator in the direction x is also positive as long as the inductance L is increasing in the same direction. Thus, the mechanical force acts in the same direction, which also increases the magnetic circuit inductance.

The mechanical force can also be calculated by changing the magnetic circuit reluctance with position. If the linkage flux λ is constant, then the flux φ in the magnetic circuit with the reluctance $\Re$ is also constant and, therefore, the mechanical force is given by the equation

$$W_{fe} = \frac{\Re\varphi^2}{2} \Rightarrow f_{em} = -\frac{\varphi^2}{2}\frac{d\Re}{dx}. \tag{5}$$

This mechanical force f_{em} acts in a direction that displaces the actuator for a geometric configuration that corresponds to the path with lowest reluctance. SR actuators base their functioning on this basic principle.

We can also define the co-energy W'_{fe} as

$$W'_{fe}(i,x) = i\lambda - W_{fe}, \tag{6}$$

depending on current i and position x,

$$dW'_{fe}(i,x) = \frac{\partial W'_{fe}(i,x)}{\partial i}di + \frac{\partial W'_{fe}(i,x)}{\partial x}dx. \tag{7}$$

Taking into account that i and x are independent variables, the linkage flux λ, inductance L and the mechanical force f_{em} can be obtained from the device co-energy map:

$$\begin{cases} \lambda = \frac{\partial W'_{fe}(i,x)}{\partial i} \Rightarrow L = \frac{\lambda}{i} \\ f_{em} = \frac{\partial W'_{fe}(i,x)}{\partial x} \end{cases}. \tag{8}$$

Thus, as can be seen, if a change in the linkage flux occurs, the system energy will also change. This variation can be promoted by means of an excitation variation, a mechanical displacement, or both. The coupling field can be understood as an energy reservoir that receives energy from the input system, in this case the electrical system, and delivers it to the output system, in this case the mechanical system.

The actuator presented here has a longitudinal configuration. A magnetic yoke and respective coil constitute each actuator phase, being each phase magnetically independent from the others. This characteristic leads to one major advantage, i.e. the flux is completely independent for each phase. This is important, because it allows the simultaneous activation of two or more phases without loss of performance due to saturation; and

increase in the number of phases is possible, which increase the smoothness of motion. The physical structure of the developed actuator is presented in Figure 2, and dimensions are listed in Table I. Each phase coil has 1100 turns and a resistance of 10 Ω.

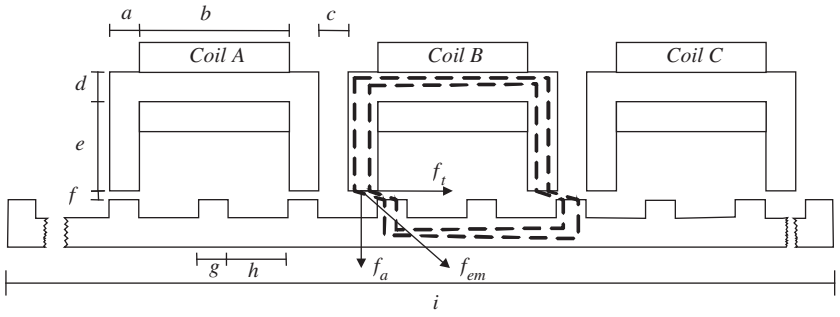

Figure 2. LSR actuator physical dimensions.

Table 1. LSRA Physical Dimensions (in millimetre units).

Yoke pole width (a)	10
Coil length (b)	50
Space between phases (c)	10
Yoke thickness (d)	10
Yoke pole depth (e)	30
Air gap length (f)	0.66
Stator pole width (g)	10
Stator slot width (h)	20
LSRA length (i)	2000
LSRA stack width	50

3. Finite element analysis

A Finite Elements (FE) model of a single-phase actuator was generated using FLUX2D [21], as shown in Figure 3. This FE model construction starts with the geometry definition, where each specific region is defined by points and lines. The FE magnetic field solution for a single-phase actuator with a phase current of 2 A can be observed in Figure 3(a). In addition, a detail of the FE mesh used to modulate the polar region is exhibited in Figure 3(b). One of the FE software features is the translation possibility of displacement, allowing the longitudinal displacement of one, or a group of regions, without needing to redefine each position of the model geometry and corresponding FE mesh. Two regions (in magenta) are defined between the groups of regions that must be moved in the longitudinal direction during static simulations. These regions are the actuator primary (in blue), the phase coil that carries current in the positive (inner region) and negative (outer region) directions (both in red), and the corresponding surrounding air (in white). Translation function demands also the definition of two narrow air-gap regions (in yellow), located in both sides of the translations regions, used for the displacement of the regions defined between them.

All regions use triangular elements in the FE generated mesh. The exceptions are the two displacement regions, which use quadrangular elements. Mesh generation must also observe that only a single layer of elements can be established in the translations air-gap regions.

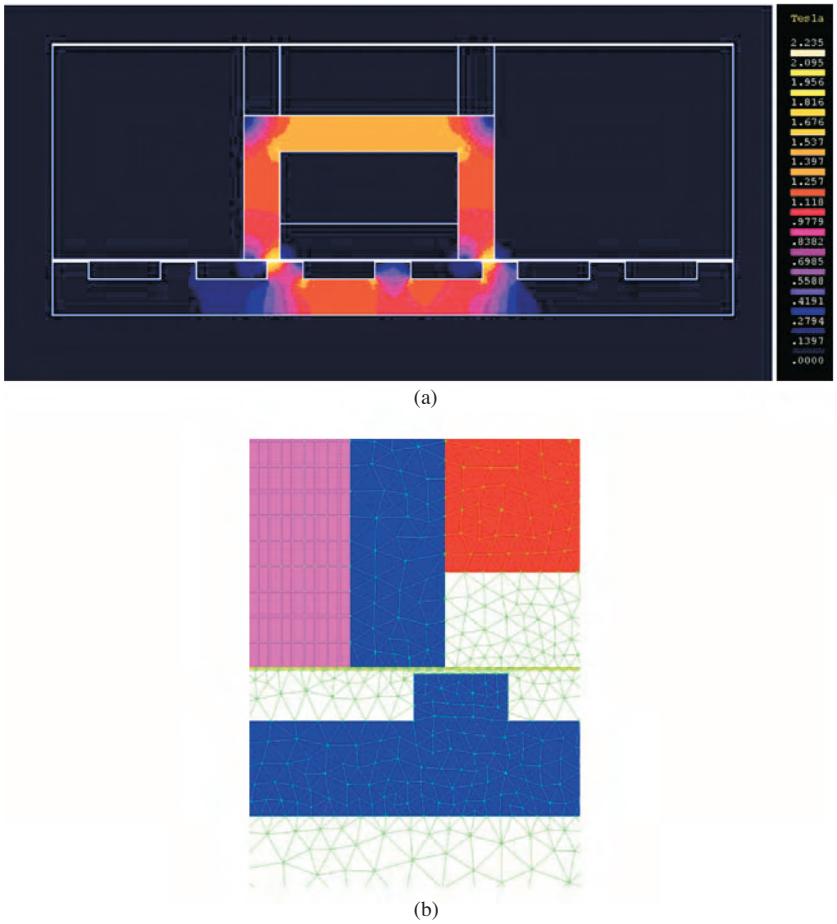

(a)

(b)

Figure 3. FE model of a single-phase actuator: a) field solution with $x = -6.66$ mm and $i = 2$ A, and b) FE mesh detail at polar region.

Actuator primary and secondary regions are both associated to materials with identical magnetic characteristics inherent to the ST-37 steel. The remaining regions inherit the magnetic characteristics of vacuum. Inside the coil regions, a current source is defined with a positive value for the region that carries the current in the positive direction, and an identical negative value for the region that carries the current in the negative direction.

Also, Dirichlet conditions are formulated in the model boundary, imposing a null flux across it. Note that the model was generated with 22351 elements.

Several simulations were performed for a set of actuator primary positions and currents. The position corresponding to the alignment between primary poles and secondary teeth is established as the reference, $x = 0$ mm. Because of the actuator repetitive geometry, the simulation only takes into consideration positions between the two unaligned configurations, $x =$ -15 mm and $x = 15$ mm. From FE simulation, the phase traction force, attraction force, energy and co-energy maps are obtained and presented in Figure 4. The obtained data are plotted as a function of actuator position and current flowing in the coil. The results are valid in the total length of the actuator, except for its extremities due to the end effects, owing to the finite length of the secondary.

As can be seen in Figure 4(a), the actuator phases are not able to develop traction force at the aligned and unaligned positions. Phases can only produce mechanical power when poles are located between the teeth of the secondary. Note that each actuator phase is able to develop a standstill traction force of almost 150 N, for a current coil equal to 4 A, obtained at the position 9 mm from the aligned position. Other characteristic aspect of the SR technology is that the developed traction force changes with position, and tries always to align the poles with the nearest secondary teeth, searching the configuration with the lowest reluctance.

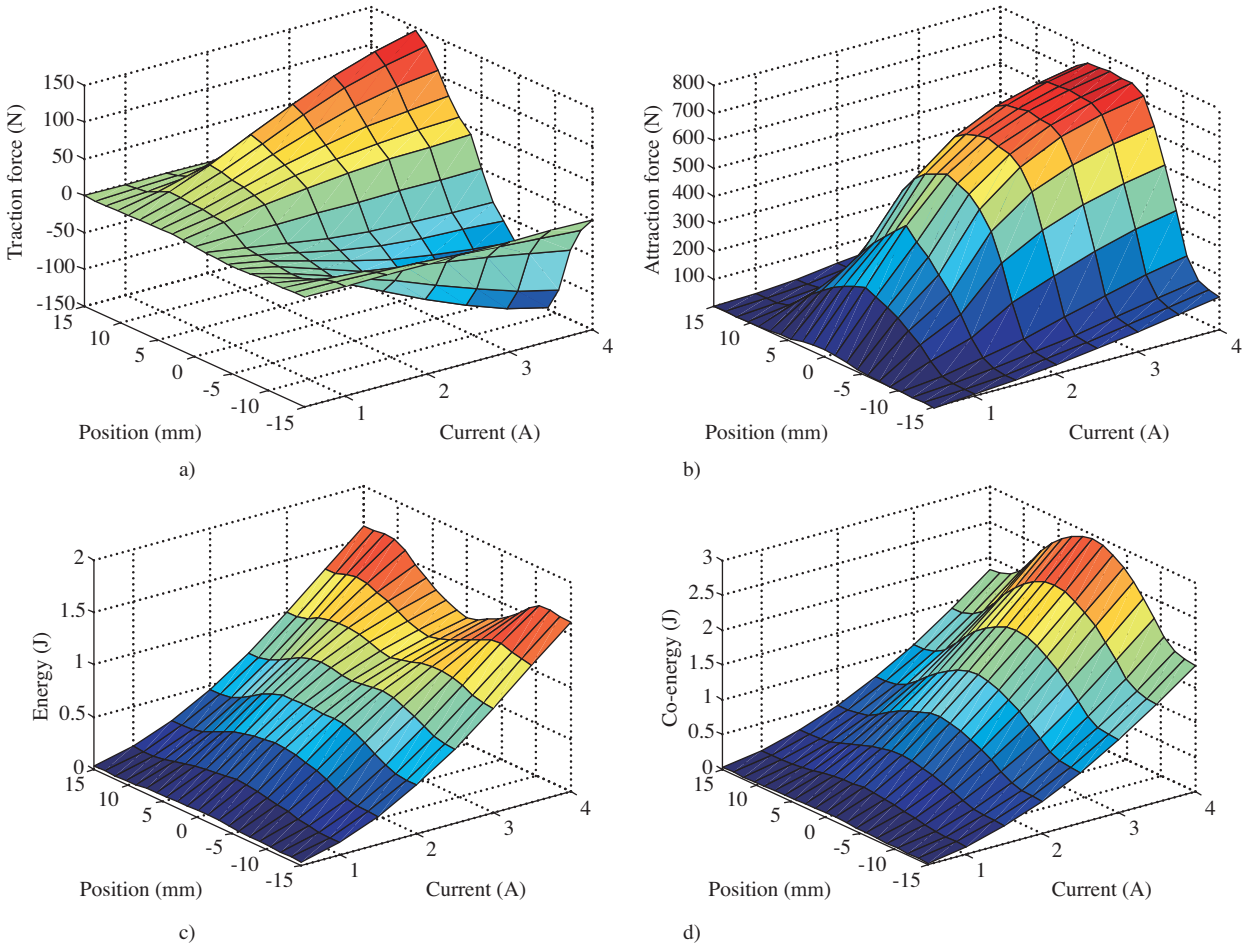

Figure 4. Actuator maps as a function of position and current for (a) traction force, (b) attraction force, (c) energy and (d) co-energy.

From the analysis of the attraction map shown in Figure 4(b), it can be observed that 750 N is approximately the maximum attraction force that an actuator phase can develop, when its coil current is 4 A, obtained at the aligned position. From the attraction force map it is also obvious a disadvantage of this geometrical configuration. When attraction force changes with position, the actuator will be subjected to an oscillatory force, perpendicular to the direction of the displacement. This will demand an extra care in the conception and construction of the structure that supports the actuator, to avoid air-gap changes. This force can be minimized introducing a different polar shape as described in [22], or then adopting a different geometrical

configuration that cancels the attraction force. For example, in a tubular configuration the resulting radial force will be null, or also in a double-side actuator the attraction force produced by one side will cancel the attraction force produced by the other.

By observing the energy map from Figure 4(c) it is notorious that the magnetic circuit starts to saturate more easily at the aligned position for currents higher than 2 A, and at this position, the reluctance is lower and, owing to that, the magnetic flux will be higher.

The higher variation of the co-energy represented in Figure 4(d) occurs in the region between aligned and unaligned positions, about 9 mm or -9 mm from the aligned position. This is coherent with the traction force map, since these are the same positions where each actuator phase is able to develop its maximum mechanical power.

The primary magnetic circuit yoke is made of three different parts, assembled together by screws. This not only enables an easy installation of the coil, but also allows the primary polar shape to change to other configurations, for example the round shape, allowing electromechanical analysis of the actuator under different polar shapes.

A support structure made of aluminium modular profiles holds up the actuator, being the secondary magnetic circuit attached to that structure by aluminium cramps. On the top of each structure side, a high precision guide rail is installed. In addition, four linear bearings, two for each side, are used to support, with aluminium cramps, the main platform that holds the actuator primary. On the other hand, the air gap length can be adjusted moving vertically the yoke to the desired position.

An encoder is coupled to the main platform, emitting two digital signals in phase quadrature, employed by the microprocessor to compute both actuator primary position and motion direction. Two linear bearings and a blocking device support an independent auxiliary platform. This platform can be blocked in a specific position with the purpose of installing the measurement equipment to perform static experiments. The actuator prototype, with primary rectangular pole shapes mounted, can be observed in Figure 5, together with the load cell used to measure the standstill developed traction force for different currents and positions.

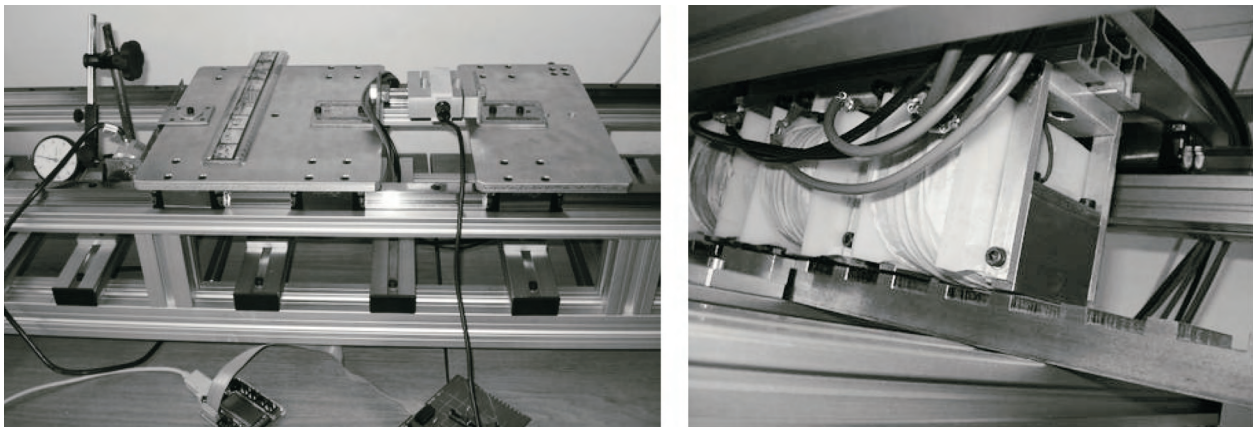

(a) (b)

Figure 5. Actuator prototype: (a) mounted in the support structure and (b) detail of the actuator primary and secondary magnetic circuits.

4. Driving electronics

The simplicity of the power converters required to supply SR actuators is one of the advantages of this technology. The power converter structure built for each phase of the developed LSRA is shown in Figure 6 [23]. It can be divided in three main blocks as follows: the Microprocessor Control System (MCS), the Regulation Electronics (RE), and the Power Electronics (PE).

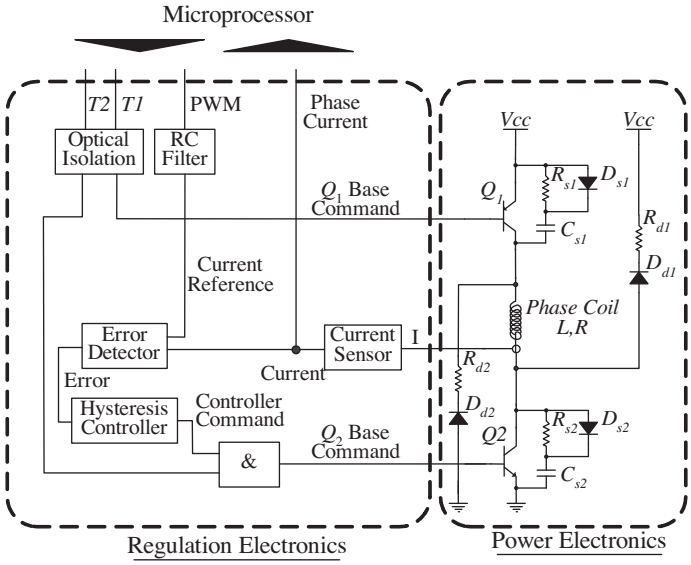

Figure 6. Power converter structure for each phase.

The PE module implements a half H-bridge. Switches Q_1 and Q_2 conducting states are commanded by Q_1 and Q_2 Base Command signals, respectively, and are protected by RCD snubbers. The half H-bridge can operate in two different freewheeling modes. If Q_2 is open then D_{d1} will turn on and current will decrease with a zero voltage applied to the phase coil. If both Q_1 and Q_2 are simultaneously turned off, then D_{d1} and D_{d2} will both turn on and current will decrease with the negative value Vcc voltage source applied to the coil. Current phase coil I is sensed by a Hall-sensor and sent to the RE module. Moreover, the PE module supports three different operating modes: soft-chopping, hard-chopping and current control.

The RE module task is to regulate the PE module operation. This action is based on the information sent to the RE module from both the microprocessor and the current sensor. After passing by a RC low pass filter, the PWM output signal delivers the Current Reference signal used to determine the Error signal used by the Hysteresis Controller, in order to drive the state of the Controller Command signal. The choice of this controller is justified because it allows the power transistors to operate in saturation state, minimizing their losses. The Q_2 Base Command signal line state results from the logic and operation between the Controller Command output and the microprocessor T_2 output. Note that if the microprocessor lines T_1 and T_2 are both high, the PWM signal reference is followed by coil current, commutating the switch Q_2. One example of operation can be observed in Figure 7, where a constant current value is obtained.

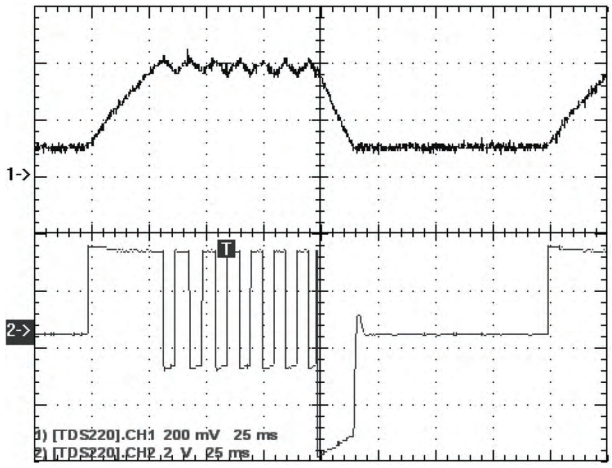

Figure 7. Phase coil current (channel 1) and voltage (channel 2).

The microprocessor can take advantage from the power drive versatility. For example, the implementation of the control strategy for the traction force will use phase position and coil current to interpolate the traction force map and decide to increase, decrease or maintain the phase current. This task can easily be performed by a microprocessor using on-chip PWM generators.

5. Position control

Two different control methodologies are proposed and evaluated as follows. The first one, the most simple, requires less computational effort, and is exclusively based on table lookup, achieving actuator primary motion with 10 mm of resolution. The second one is based on sliding mode theory, in which the traction force produced by two phases is used to move actuator primary with a resolution of 1 mm.

The LSR actuator electromagnetic model to $n = \{1, 2, 3\}$ phases is described by means of (9), where R_n the resistance of the coil, v_n the supplied voltage and i_n is the phase current. Equation (10) describes actuator mechanical behaviour, where a is the device acceleration and M its mass. Actuator nonlinearity is taken into account because both inductance $L(i,x)$ and traction force $F(i,x)$ change not only with position x, but also with current i:

$$0 = R_n i_n(t) + \frac{dL(i_n,x)i_n(t)}{dt} - v_n = \frac{di_n}{dt}\left[L(i_n,x) + i_n(t)\frac{\partial L(i_n,x)}{\partial i}\right] + \frac{dx}{dt}\left[i_n\frac{\partial L(i_n,x)}{\partial x}\right] + R_n i_n(t) - v_n \tag{9}$$

$$a = \frac{F(i,x)}{M}. \tag{10}$$

The state space is defined as

$$\begin{cases} \frac{dx}{dt} = y \\ \frac{dy}{dt} = \frac{F}{M} \\ \frac{di_n}{dt} = -\frac{y\beta_n + R_n i_n - v_n}{\alpha_n} \end{cases}, \tag{11}$$

where α_n and β_n are given by the equations

$$\begin{cases} \alpha_n = L(i_n, x) + i_n \frac{\partial L(i_n,x)}{\partial i} \\ \beta_n = i_n \frac{\partial L(i_n,x)}{\partial x} \end{cases} . \tag{12}$$

5.1. Fixed position controller

Based on position, a very simple control strategy can be implemented. Two specific positions, corresponding to the activation and inactivation of actuator phases, are defined as ***Xa_on*** and ***Xa_off***, respectively. Every time the primary reaches one of the positions listed in Table II, the microprocessor will properly manage the state of power drive inputs T1 and T2, in order to turn on or turn off each one of the three actuator phases, here designed by phase A, phase B and phase C. As can be seen in Table II, two different ways are used. The sequence *Sq1* is used to start the motion and, after that, sequence *Sq2* is used in subsequent thrust force production to maintain the movement. Motion starts with phase A positioned 10 mm away from the aligned position.

Table 2. Lookup table for phases activation.

	Phase A		Phase B		Phase C	
	Xa_on	Xa_off	Xb_on	Xb_off	Xc_on	Xc_off
Sq1	0	10	1	15	10	28
Sq2	19	30	30	45	37	56

The control strategy was implemented on a MSP430F449 device, taking advantage of its on-chip timers and digital IO. One of the two encoder signals generates an interrupt at each rising edge, and the interrupt service routine reads the other line to determine if the position counter must be increased or decreased. Timer A is used to generate the PWM needed to control the current, and Timer B is used with the compare/capture units to generate the signal pattern to drive the power converter as represented in Figure 8.

The following results were obtained from a two working sequences A-B-C, representing six traction force pulses. As can be seen in Figure 9, actuator nearly reaches a velocity of 300 mm/sec. After the last pulse, the velocity decreases linearly.

It can be observed in Figure 10 that this driving scheme only allows movements with a resolution of 10 mm. During the laboratory tests, the primary of the actuator moved 90 mm, that is, it stopped when the phase C was aligned.

5.2. Sliding mode controller

Variable Structure Systems (VSS) belong to a particular case of automatic control systems [24–26]. Intentional commutation is introduced between two different control actions, in one or more channels of control inputs. Considering the nonlinear dynamical system described by

$$\dot{X} = A(X, t) + B(X, t)u, \tag{13}$$

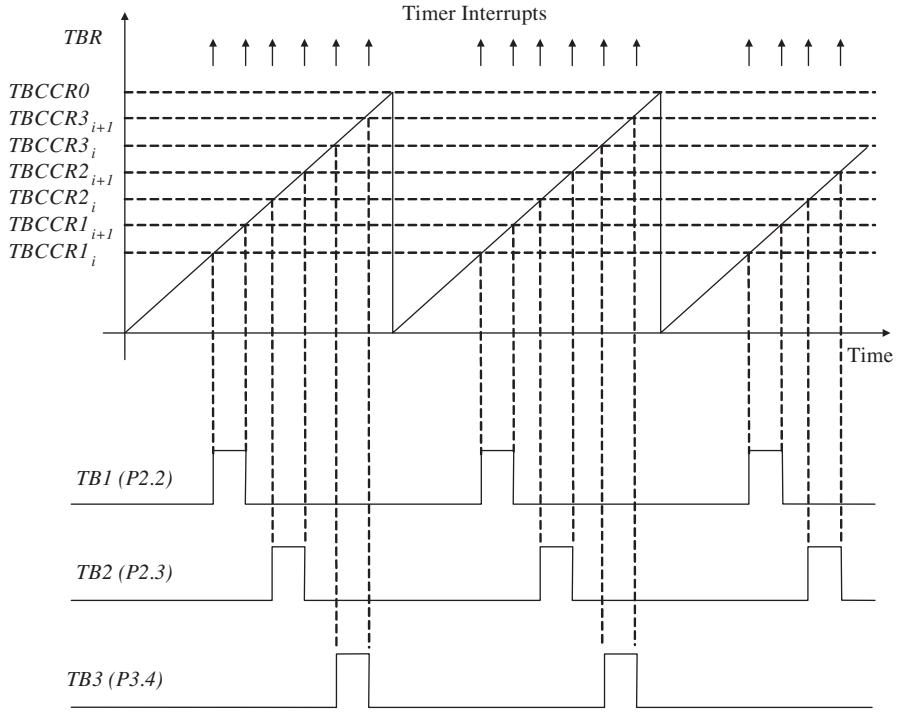

Figure 8. Power converter pattern output.

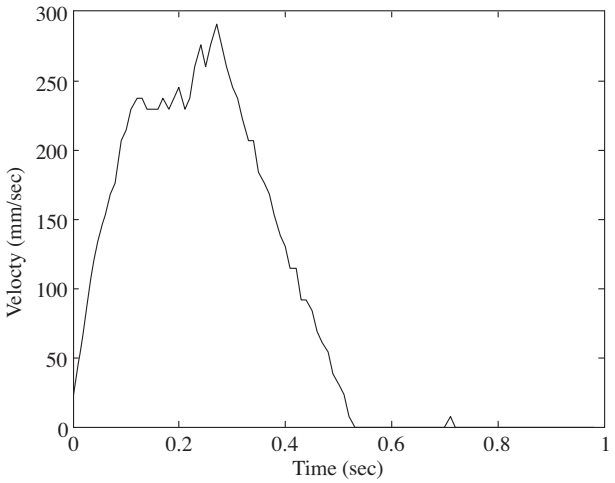

Figure 9. Actuator velocity.

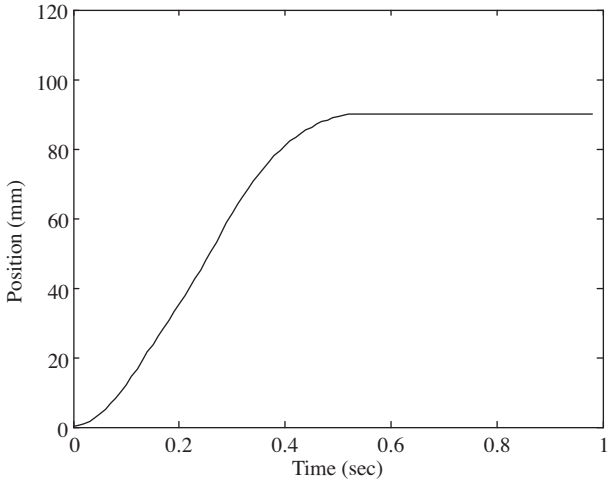

Figure 10. Actuator position.

the possible type of motion of a VSS in the state space is manifested by the appearance of the sliding mode regime. To achieve this regime, a switching surface is defined by $s(X,t) = 0$, where the control structure $u(X,t)$ stated in (14) changes from one structure to another. When $s(X,t) > 0$ the variable structure control is changed in order to decrease $s(X,t)$, and the same kind of action is performed when $s(X,t) < 0$. The control main goal is to keep the system state space sliding in the surface $s(X,t) = 0$. During this sliding motion, the system behaves like a reduced-order system, being insensitive to disturbances and parameters changes. Control structure can be expressed by the system

$$u(X,t) = \begin{cases} u^{+}(X,t) & \Leftarrow \quad s(X) > 0 \\ u^{-}(X,t) & \Leftarrow \quad s(X) < 0 \end{cases} . \tag{14}$$

The previously explained concept is used to develop the LSR actuator position structure control. At a specific moment, it is assumed that traction force can be developed in both directions with suitable actuator phase choice. After turning off, an actuator phase still has the ability to produce traction force. This situation occurs because current phase does not go down instantaneously, but diminishes by the freewheeling diodes path, with a time constant that depends on phase inductance and resistance. This behaviour is responsible for the introduction of a delay in the controller response, contributing to increase the oscillations (chattering) around the sliding surface.

Actuator movement can be expressed as a VSS with two possible control actions. One of them produces a traction force towards the left direction $F_l(i,x)$, while the other produces a traction force towards the right direction $F_r(i,x)$. These control actions are derived from the traction force. As was explained previously, this force is not constant, and changes in time with position and current. Despite this detail, the two control actions successfully manage to drive the system through the sliding line, reaching the origin of the phase plane:

$$\begin{cases} \dot{x} = y \\ \dot{y} = \frac{u}{M} \end{cases} . \tag{15}$$

The control law $u(t)$ is established as

$$u(t) = \begin{cases} F_r(i,x) & \Leftarrow \quad s(e,\dot{e}) > 0 \\ F_l(i,x) & \Leftarrow \quad s(e,\dot{e}) < 0 \end{cases} . \tag{16}$$

The commutation function $s(e,\dot{e})$ depends on position error e and derivative of the position error $\dot{e}$, and is defined by

$$s(e,\dot{e}) = me + \dot{e}, \tag{17}$$

where m is a positive constant, experimentally obtained, and here equal to 0.5.

The controller selects, from the lookup Table III, the phase that will provide the desired control action, in order to maintain $s(e,\dot{e}) = 0$. The aligned position for phase A is taken as reference.

Table 3. Relative actuator position (in millimetre units).

Traction force	[0,10[	[10,20[	[20,30[
Left direction (F_l)	Phase A	Phase B	Phase C
Right direction (F_r)	Phase B	Phase C	Phase A

The TMS320F2812 eZdsp Start Kit was used to implement and apply to the LSRA, the proposed control strategy, based on sliding mode control, and Event Manager EVA was used to generate the PWM signal dedicated to each phase current acquired by the on-chip ADC. Velocity and position are derived from the QEP unit based on encoder signals.

The sliding mode controller establishes the switching strategy to be used to turn on and turn off the LSR actuator phases by means the microcontroller GPIO. The most important software blocks are shown in Figure 11.

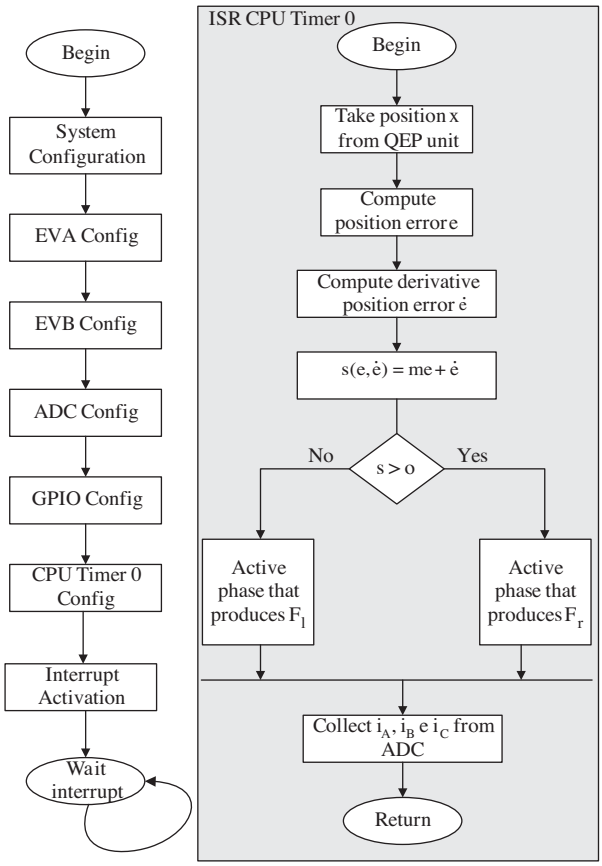

Figure 11. TMS320F2812 eZdsp Start Kit code flow.

Experimental results obtained from several small displacements for a starting position corresponding to the alignment between phase C poles and secondary teeth can be seen in Figure 12, where the chattering

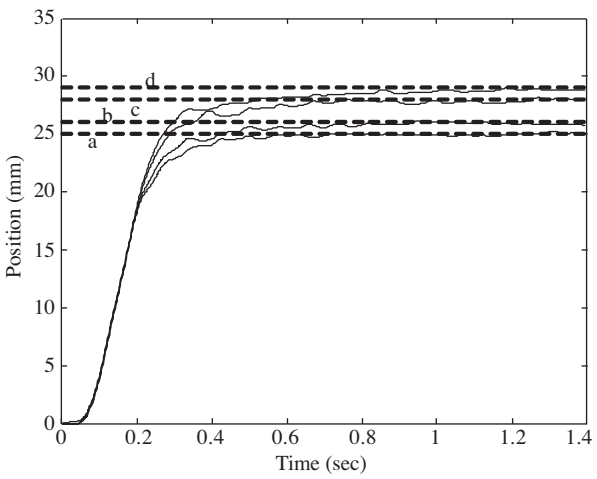

Figure 12. Actuator position for small displacements: (a) 25 mm, (b) 26 mm, (c) 28 mm, (d) 29 mm.

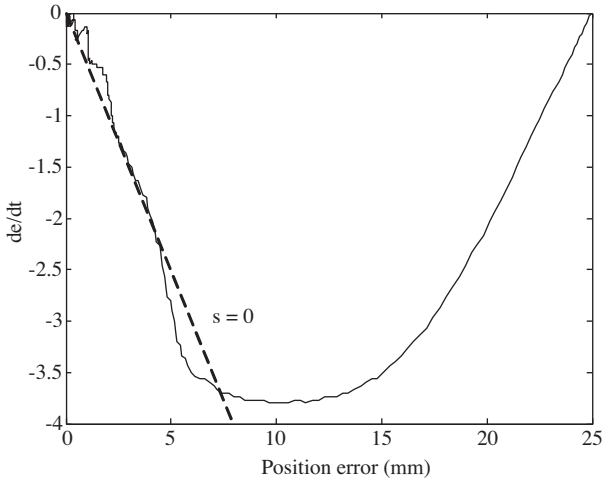

Figure 13. Phase portrait for a 25 mm displacement.

introduced by the sliding mode control action can be observed at steady state. The phase portrait trajectory along the sliding line to the origin can be observed in Figure 13, for a specific situation corresponding to a 25 mm displacement.

6. Conclusions

The key aspects concerning the development of a linear switched reluctance actuator have been presented. The working principle and the theoretical background were introduced. In addition, a finite element model was constructed based on a finite element tool used to perform an actuator analysis. The obtained results allowed to plotting device characteristic maps for several stationary physical quantities, like traction and attraction forces, energy and co-energy. Based on the obtained results an experimental prototype was also constructed. Each phase from the proposed actuator is able to develop a standstill traction force of 150 N of with a field current of only 4 A.

The most advisable power drive to supply the actuator phases, under supervision of a microcontroller, was also presented and described. The proposed hardware can be used with different operating modes such as single pulse, soft-chopping or hard-chopping. On the other hand, the on-board hardware hysteretic control loop can be used to assure a specific current profile or control the developed traction force without direct interference of the microcontroller.

The actuator behaviour was experimentally verified under two different control methods. The first control method turns on and off actuator phases at specific positions. Two tables are used to save in memory the activation and deactivation positions. One table is used to start the movement, while the other is used after the first sequence of thrust pulses. This control strategy allows to move the actuator with a maximum resolution equal to the polar width (10 mm). The polar width can be decreased to increase actuator resolution, but this will have consequences in the traction force. The second control mechanism was based on a sliding mode strategy. Two phases were simultaneously used to produce a force that will cancel the position error. The best results had been obtained with this control methodology. Small displacements with resolution of 1 mm had been experimentally observed.

The obtained results show that the linear switched reluctance actuator can be used in positioning tasks. Its low cost and reliability make it very attractive in the industrial field application.

References

[1] A. Cassat, N. Corsi, R. Moser, N. Wavre, “Direct Linear Drives: Market and Performance Status,” Proceedings of the 4th International Symposium on Linear Drives for Industry Applications, LDIA2003, pp. 1-11, 8-10 September 2004.

[2] L. Li, S. Aoyagi, Y. Arai, N. Tagawa, “Development of composite multi-layered PZT thin films for microactuator,” Proceedings of the IEEE International Symposium on Industrial Electronics, ISIE 2007, pp. 1478-1481, 4-7 June 2007.

[3] Federico Carpi, Danilo De Rossi, “Electroactive polymer based devices for e-textiles in biomedicine,” IEEE Transactions on Information Technology in Biomedicine, Vol. 9, No. 3, pp. 295-318, September 2005.

[4] Byungkyu Kim, Sunghak Lee, Jong Heong Park, Jong-Oh Park, "Design and Fabrication of a Locomotive Mechanism for Capsule-Type Endoscopes Using Shape Memory Alloys (SMAs)," EEE/ASME Transactions on Mechatronics, Vol. 10, No. 1, pp. 77-86, February 2005.

[5] Hiroyuki Fujita, Akito Omodaka, "The Fabrication of an Electrostatic Linear Actuator by Silicon Micromachining," IEEE Transactions on Electron Devices, Vol. 35, No. 6, pp. 731-734, June 1988.

[6] Siyuan He, Ridha Ben Mrad, "Large-Stroke Microelectrostatic Actuators for Vertical Translation of Micromirrors Used in Adaptive Optics," IEEE Transactions on Industrial Electronics, Vol. 52, No. 4, August 2005.

[7] E.R. Laithwaite, "Adapting a linear induction motor for the acceleration of large masses to high velocities," IEE Proc. Electr. Power Appl., Vol. 142, No. 4, pp. 262-268, July 1995.

[8] Lucian N. Tutelea, Myung Chin Kim, Marcel Topor, Ju Lee, Ion Boldea, "Linear Permanent Magnet Oscillatory Machine: Comprehensive Modeling for Transients with Validation by Experiments," IEEE Transactions on Industrial Electronics, Vol. 55, No. 2, pp. 492-500, February 2008.

[9] Ying-Shieh Kung, "Design and Implementation of a High-Performance PMLSM Drives Using DSP Chip," IEEE Transactions on Industrial Electronics, Vol. 55, No. 3, pp. 1341-1351, March 2008.

[10] Mahesh Krishnamurthy, Chris S. Edrington, Ali Emadi, Peyman Asadi, Mehrdad Ehsani, Babak Fahimi, "Making the Case for Applications of Switched Reluctance Motor Technology in Automotive Products," IEEE Transactions on Power Electronics, Vol. 21, No. 3, pp. 659-674, May 2006.

[11] Ibrahim H. Al-Bahadly, "Examination of a Sensorless Rotor-Position-Measurement Method for Switched Reluctance Drive," IEEE Transactions on Industrial Electronics, Vol. 55, No. 1, pp. 288-295, January 2008.

[12] CHAI J. Y., LIN Y. W., LIAW C. M., "Comparative study of switching controls in vibration and acoustic noise reductions for switched reluctance motor," Proceedings of IEE Proceedings of Electric Power Applications, Vol. 153, No. 3, pp. 348-360, May 2006.

[13] Hao CHEN, Xiaohui QIU, Yang ZHAO, "Conductive EMI noise measurement for switched reluctance drive," Turkish Journal of Electrical Engineering & Computer Sciences, Vol. 17, No. 3, 2009.

[14] Hao Chen, Zuo Shao, Yifeng Zhu, "Rotor Speed Testing and Closed-loop Control for Switched Reluctance Motor Drive Based on Fuzzy Logic," Proceedings of WCICA – Fifth World Congress on Intelligent Control and Automation, Vol. 5, pp. 4458-4462, 2004.

[15] Hao Chen, Yifeng Zhu, "Torque Control of Switched Reluctance Machine Drive System," Proceedings of ICEMS - Sixth International Conference on Electrical Machines and Systems, Vol. 2, pp. 895-898, 2003.

[16] Gobbi R., N.C. Sahoo, M.K.A. Ahamed Khan, "A Fuzzy Logic Based Current Modulation for Torque Ripple Minimization in Switched Reluctance Motors," Proceedings of PECon - National Power & Energy Conference, pp. 46-51, 2004.

[17] H. S. Lim, R. Krishnan, and N. S. Lobo, "Design and Control of a Linear Propulsion System for an Elevator Using Linear Switched Reluctance Motor Drives," IEEE Transactions on Industrial Electronics, Volume 55, No. 2, pp. 534-542, February 2008.

[18] Ge Baoming, Aníbal T. de Almeida, Fernando J. T. E. Ferreira, "Design of Transverse Flux Linear Switched Reluctance Motor," IEEE Transactions on Magnetics, Vol. 45, No. 1, January 2009.

[19] Liu Yuan-Jiang, G.P.Widdowson, S.Y.Ho, Gan Wai Chuen, P. Borsje, "Design and Analysis of Linear Switched Reluctance Motor for High Precision Position Control," Proceedings of Electric Machines & Drives Conference, Volume 1, pp. 55-58, 2007.

[20] Shi Wei Zhao, Norbert C. Cheung, Wai-Chuen Gan, Jin Ming Yang, Jian Fei Pan, "A Self-Tuning Regulator for the High-Precision Position Control of a Linear Switched Reluctance Motor," IEEE Transactions on Industrial Electronics, Vol. 54, No. 5, pp. 2425-2434, October 2007.

[21] Flux2D Tutorial (Version 7.40), Cedrat, August, 1999.

[22] A. Espírito Santo, M. R. Calado, C. M. Cabrita, "Finite Elements Analysis of Linear Switched Reluctance Actuator Pole and Teeth Shape," Proceedings of the XIII International Symposium on Electromagnetic Fields in Mechatronics, Electrical and Electronic Engineering, September 2007.

[23] A. Espírito Santo, M. R. Calado, C. M. Cabrita, "Power Converter For a Linear Switched Reluctance Actuator With Hysteresis Current Controller," Proceedings of the International Conference on Power Engineering, Energy and Electrical Drives, pp. 336-341, April 2007.

[24] John Y. Hung, Weibing Gao, James C. Hung, "Variable Structure Control: A Survey," IEEE Transactions on Industrial Electronics, Vol. 40, No 1, pp. 2-22, February 1993.

[25] Raymod A. DeCarlo, Stanislaw H. Zak, Gregory P. Matthews. "Variable Structure Control of Linear Multivariable Systems: A Tutorial," Proceeding of the IEEE, Vol. 76, No 3, March 1988.

[26] K. David Young, Vadim I. Utkin, Umit Ozguner. "A Control Engineer's Guide to Sliding Mode Control," IEEE Transactions on Control Systems, Vol. 7, pp. 328-342, May 1999.